STUDYING THE MECHANICS OF MEMBRANE PERMEABILIZATION THROUGH MECHANOELECTRICITY

Joyce El-Beyrouthy[1], Michelle M. Makhoul-Mansour[1], Eric C. Freeman[1]*

[1]School of Environment, Civil, Agriculture and Mechanical Engineering. The University of Georgia, Athens, GA, 30602, United States

*Corresponding Author: ecfreema@uga.edu

Biomembranes Engineering Laboratory

School of Environmental, Civil, Agricultural and Mechanical Engineering

The University of Georgia

Athens, GA 30602

KEYWORDS: Droplet interface bilayer; electrophysiology; mechanoelectricity; membrane electrostatics; transient surface interactions.

ABSTRACT. In this research real-time monitoring of lipid membrane disruption is made possible by exploiting the dynamic properties of model lipid bilayers formed at oil-water interfaces. This involves tracking an electrical signal generated through rhythmic membrane perturbation translated into adsorption and penetration of charged species within the membrane. Importantly, this allows for the detection of membrane surface interactions that occur prior to pore formation that may be otherwise undetected. The requisite dynamic membranes for this approach are made possible through the droplet interface bilayer (DIB) technique. Membranes are formed at the interface of lipid monolayer-coated aqueous droplets submerged in oil. We present how cyclically alternating the membrane area leads to the generation of mechanoelectric current. This current is negligible without a transmembrane voltage until a composition mismatch between the membrane monolayers is produced, such as a one-sided accumulation of disruptive agents. The generated mechanoelectric current is then eliminated when an applied electric field compensates for this asymmetry, enabling measurement of the transmembrane potential offset. Tracking the compensating voltage with respect to time then reveals gradual accumulation of disruptive agents prior to membrane permeabilization. The innovation of this work is emphasized in its ability to continuously track membrane surface activity, highlighting the initial interaction steps of membrane disruption. In this manuscript we begin by validating our proposed approach against measurements taken for fixed composition membranes using standard electrophysiological techniques. Next, we investigate surfactant adsorption, including hexadecyltrimethylammonium bromide (CTAB, cationic) and sodium decyl sulfate (SDS, anionic), demonstrating the ability to track adsorption prior to disruption. Finally, we investigate the penetration of lipid membranes by melittin, confirming that the peptide insertion and disruption mechanics are in-part modulated by membrane composition.

INTRODUCTION. Cellular membranes are semi-permeable lipid bilayers enclosing the intracellular components and isolating the cytosol from the extracellular environment, essential for healthy cellular functionality [1]. This protective barrier regulates transport of dissolved species into and out of the cell, making it the first point of interaction between a targeting agent and the desired cells [2, 3]. Characterizing the mechanics between dispersed species in aqueous environments and cellular membranes is key for understanding agent-aided cellular activities, such as the functionalities of peptides [1] and the development of drug delivery systems [4]. Peptides interactions are either membrane-permeabilizing or non-permeabilizing, where the latter consists of the biomolecules crossing the membrane without significant disruption [1]. Furthermore, the development of synthetically formulated nanoparticles such as biodegradable nanocarriers [5], antimicrobial polymers [1], and detergents [6, 7] requires a deep understanding of the membrane-agent mechanics. In fact, targeted functional design for membrane interactions such as drug delivery vectors requires a careful balance between efficacy and cytotoxicity [4, 8], and thus better characterization of their interactions with the lipid membrane is necessary. Herein, we proposes a novel technique to test these interactions and characterize the membrane disruption process in the design of pharmaceuticals [4], nanoparticles [9] and materials engineering [9, 10].

Cellular membranes are fundamentally structured as double layers of phospholipids possessing a hydrophobic interior and two hydrophilic outer layers [11]. The bulk membrane properties are largely dictated by the lipid composition and organization within the membrane. For example, the exoplasmic leaflet of gram bacteria presents a negative surface charge from the abundant presence of anionic headgroups, rendering them more susceptible to cationic antibacterial agents [12]. These properties are the driving forces for nonselective membrane surface interactions, such as micelle-forming detergents and some cationic antimicrobial peptides [1, 13]. These nonselective

interactions are mediated by a combination of properties of the disruptive agent and the membrane. Electrostatic forces attract positively charged species to a typically negatively-charged membrane surface where initial attachment occurs, followed by membrane penetration through hydrophobic affinity [1]. These types of interactions are the main focus of this work, where alterations in the membrane electrostatic profile are tracked.

Membrane disruption mechanics are often studied in a controlled environment through the formation of model lipid membranes. These lipid membranes mimic the fundamental structure of biological membranes and contain a double layer of phospholipids, produced *in vitro* through a variety of methods [14]. Model membranes present a simplified yet tunable architecture, providing a repeatable, and adjustable platform for investigating membrane interactions through various approaches [15-17]. For example, super-resolution microscopy allows for the characterization of lipid domains [18], interferometry has been utilized to observe real-time binding of proteins to liposomes [19] and X-ray and neutron techniques allow for the characterization of functional nanoparticles with planar supported model membranes [20]. Combining two techniques largely enhances their advantages, such as combining AFM (atomic force microscopy) and X-ray reflectivity provides simultaneous structure and electrostatic characterization [21], or using optical trapping with confocal Raman spectra allows for longer data acquisition period [22]. Furthermore, computational simulations provide an indispensable tool to predict the behavior of these interactions on a molecular level [23, 24].

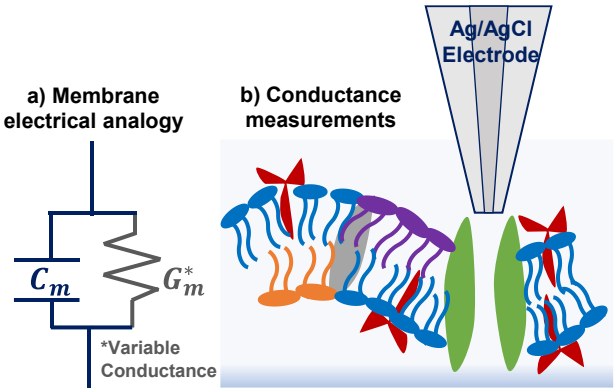

Figure 1. a) Membrane electrophysiology enables the investigation of membrane active agents, through membrane electrical representation: a capacitor and a resistor in parallel. b) The introduction of a membrane-solubilizing agent leads to changes in these properties, driven by the formation of pores, or conductive pathways, allowing ionic transport across the double layer. Traditional electrophysiology studies focus on tracking the dynamic changes in membrane conductance to reveal information about the adsorption mechanism and the model of pore formation. Ag/AgCl electrodes allow for controlling the voltage drop across the membrane while measuring the corresponding generated current.

Herein we propose a new technique for tracking membrane-agent interactions prior to permeabilization. This technique is based on membrane electrophysiology for understanding membrane-agent interactions. Electrophysiology relies on monitoring changes in the bilayer's electrical properties [14, 25-28], where the membrane is approximated as a capacitor and a resistor in parallel [25, 29, 30] as illustrated in **Figure 1.** The membrane capacitance arises due to the difference in hydrophilic-hydrophobic permittivity of the lipid regions [29, 31], whereas its resistance is a result of its well-packed hydrophobic interior. Changes in these properties are used to detect membrane activity [32]. The commonly adopted approach is tracking changes in membrane conductance as the latter varies in response to membrane permeabilization [25, 33].

Sudden changes in the membrane conductance signify the formation of pores within the membrane, and the characteristics and intensity of these events are used to describe the pore-forming mechanism [25]. However, these measurements typically capture the point at which pores are generated rather than providing insights into interactions prior to permeabilization such as the accumulation within the membrane.

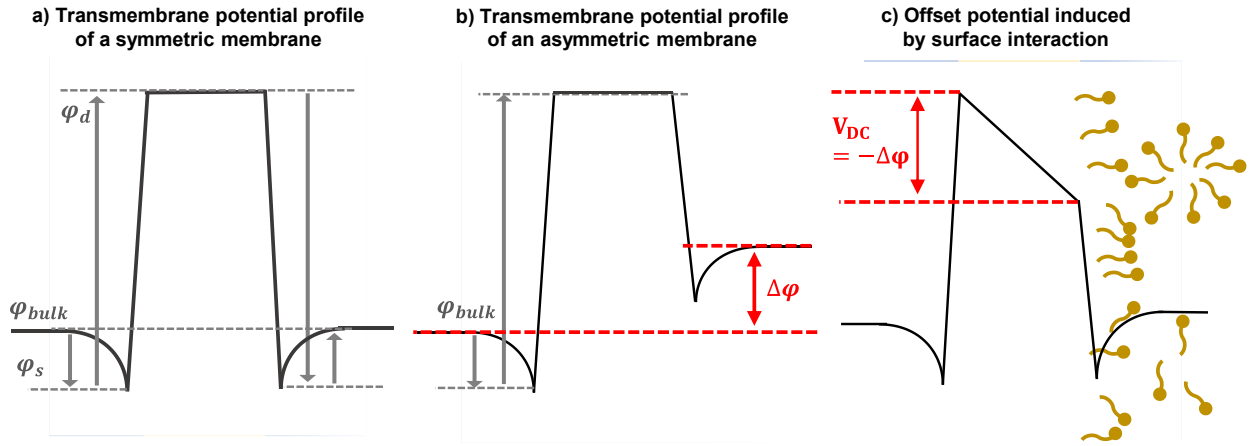

Figure 2. Lipid monolayers possess a surface, $\boldsymbol{\varphi_s}$, and a dipole, $\boldsymbol{\varphi_d}$, potential. The amplitude and distribution of these potentials outline the transmembrane potential profile. a) In the case of monolayers formed from the same lipid mixtures, the membrane is called symmetric, and these potentials are well-balanced across the double layer. b) In the case where monolayers are formed from different lipid compositions, the membrane is called asymmetric, and the potential profile shows an imbalance, denoted as the membrane potential offset, $\Delta\varphi$. c) This offset may also be variable if induced by an unequal and fluctuating adhesion of disruptive agents across the membrane. In all cases, membrane potential offset can be compensated for through the introduction of an external electric field reestablishing the charge distribution and membrane symmetry.

The technique proposed herein expands on the capacitor-resistor model of the membrane, and focuses on localized electric fields within the membrane interior [34]. Phospholipids are amphiphilic molecules possessing a specific charge distribution across their molecular structure, which leads to localized potentials within the lipid leaflets, including surface (φ_s) and dipole (φ_d) potentials [29]. The surface potential depends on the leaflet surface charge governed by the phospholipids headgroup interactions with the surrounding electrolyte solution [35], whereas the dipole potential arises due to dipolar residues at the linking group of the amphiphilic molecule [36]. The amplitude and distribution of these localized potentials across the two lipid layers dictate the overall transmembrane potential profile illustrated in **Figure 2.** In the case where the two leaflets are formed from the same lipid compositions, the identical surface and dipole potentials produce a symmetric transmembrane potential profile as illustrated in **Figure 2 (a).** In the case where the membrane leaflets are formed with different lipid compositions, the dissimilarity between the potentials generates an imbalance across the membrane profile, as presented in **Figure 2 (b).** When the membrane is short-circuited through electrodes placed in the neighboring solution, this imbalance in potentials combined with a prescribed bulk potential produces an offset in the transmembrane electric field, denoted as membrane potential offset, $\Delta\varphi$ [37]. Previous electrophysiology analyses [29, 38] showed that it is possible to compensate for this offset by applying a matching voltage at the boundaries, as represented by the dashed lines of **Figure 2 (c),** eliminating the total field across the membrane. This compensating voltage is equivalent to the membrane potential offset, and resolving this value provides measurements for the developing membrane asymmetry.

The membrane potential offset is often measured using the minimum capacitance technique based on electrowetting principles [39, 40]. This method is reliable and accurate and has been

successfully applied to many studies of membrane asymmetry [39, 41, 42]. However, the membrane must reach its equilibrium dimensions for each voltage to produce the desired quadratic trend [40]. Consequently the frequency of the measurement is often insufficient to resolve membrane-agent interactions [6]. An alternative approach is necessary for the analysis of developing changes in the membrane structure. The use of the intramembrane field compensation technique allows for investigating dynamic membrane mechanics through electrocompression [43-46]. This technique works best with softer model membranes exhibiting a higher degree of thinning under an applied voltage [46, 47].

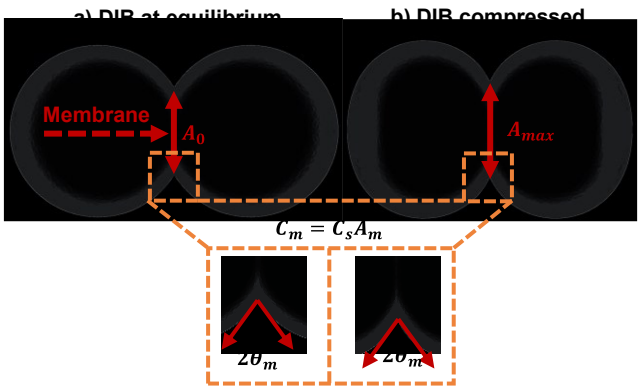

Figure 3. A model for droplet compression. The droplet interface bilayer, or DIB, is a model membrane formed at the interface of two lipid monolayer-coated droplets in an oil medium. a) At equilibrium, the membrane area is at its resting initial value minimizing the system's total energy. b) The DIB setup allows for the displacement of one droplet with respect to the other, causing the membrane area to oscillate. Due to the area-capacitance relationship of lipid membranes, these oscillations lead to the generation of a capacitive-current: mechanoelectricity. Images are produced using the Surface Evolver computational software for predicting equilibrium droplet shapes with varying constraints [48, 49].

The presented approach is based on the droplet interface bilayer (DIB) as the model membrane [50, 51]. As modeled in **Figure 3 (a)**, DIBs form lipid membranes at the interface of two lipid-coated aqueous droplets in an oil medium. These emulsion-based systems are advantageous as they allow for the creation of asymmetric membranes [39, 41] as well as tunable membrane areas [40, 47] through compression [52] as depicted in **Figure 3 (b)**. Alternating the membrane area through harmonic compression combined with an electric field across the membrane produces capacitive currents [40, 47]. This capacitive-induced current is denoted as the mechanoelectric current and assuming negligible membrane leak, the equation describing it is as follows [52]:

$$I(t)_{mech} = (V_{DC} + \Delta\varphi)\frac{dC(t)}{dt} \quad (1),$$

where $I(t)_{mech}$ is the mechanoelectric current, V_{DC} is the applied direct voltage, $\Delta\varphi$ is the membrane potential offset and $C(t)$ is the alternating change in membrane capacitance. Notably, $I_{mech} = 0$ when $V_{DC} = -\Delta\varphi$, minimizing the current when the applied direct voltage balances any offset generated by membrane asymmetry.

This work utilizes **Equation (1)** as the fundamental link for characterizing membrane asymmetry through mechanoelectricity. The necessary voltage for eliminating the mechanoelectric current is set to be equal in magnitude and opposite in sign to the potential offset. The Grahame equation is then used to approximate the corresponding surface charge when desired, requiring the assumption of minimal agent translocation across the membrane [53].

We examine the mechanoelectric approach in several steps, first validating the technique against other methods then extending to new capabilities. To begin, results for quasi-fixed voltage offsets produced through membrane asymmetry are compared against results from the minimum capacitance technique. Afterwards, mechanoelectricity is used to characterize micelle-forming detergents CTAB (hexadecyltrimethylammonium bromide) and SDS (sodium dodecyl sulfate) to

demonstrate tracking of membrane-detergent interactions. These agents are selected as they have been thoroughly studied with model membranes providing a basis for evaluating our approach [54, 55]. Following, surface charge dependent interactions of the membrane-permeabilizing peptide, melittin were investigated. Melittin is a membrane-active cationic antimicrobial peptide that interacts differently with zwitterionic and anionic membranes [56-59]. We use melittin's dependency on membrane composition to further demonstrate applications of the mechanoelectricity technique by examining surface accumulation prior to pore formation for varying membrane surface charges.

EXPERIMENTAL APPROCH. This section briefly discusses the experimental apparatus used for generating and minimizing the mechanoelectric current. Additional experimental details and results are provided in the supplementary information document as follows: **Section S.1** Lipids and Agents Solution Preparations; **Section S.2** Freely Hanging Droplet Interface Bilayers and The Minimum Capacitance Technique; **Section S.3** Surface Charge Calculations; **Section S.4** Mechanoelectricity Setup and Optimization; **Section S.5** Fixed Potential Offset Measurement; **Section S.6** Resolving Lipid Flip-Flop in Static Membranes; **Section S.7** Membrane-Agent Dynamic Studies; **Section S.8** Diffusion in the Droplet Observed Through Calcein; **Section S.9** Full Detergents Results; and **Section S.10** Full Melittin Results.

MECHANOELECTRC CURRENT GENERATION AND CALCULATION.

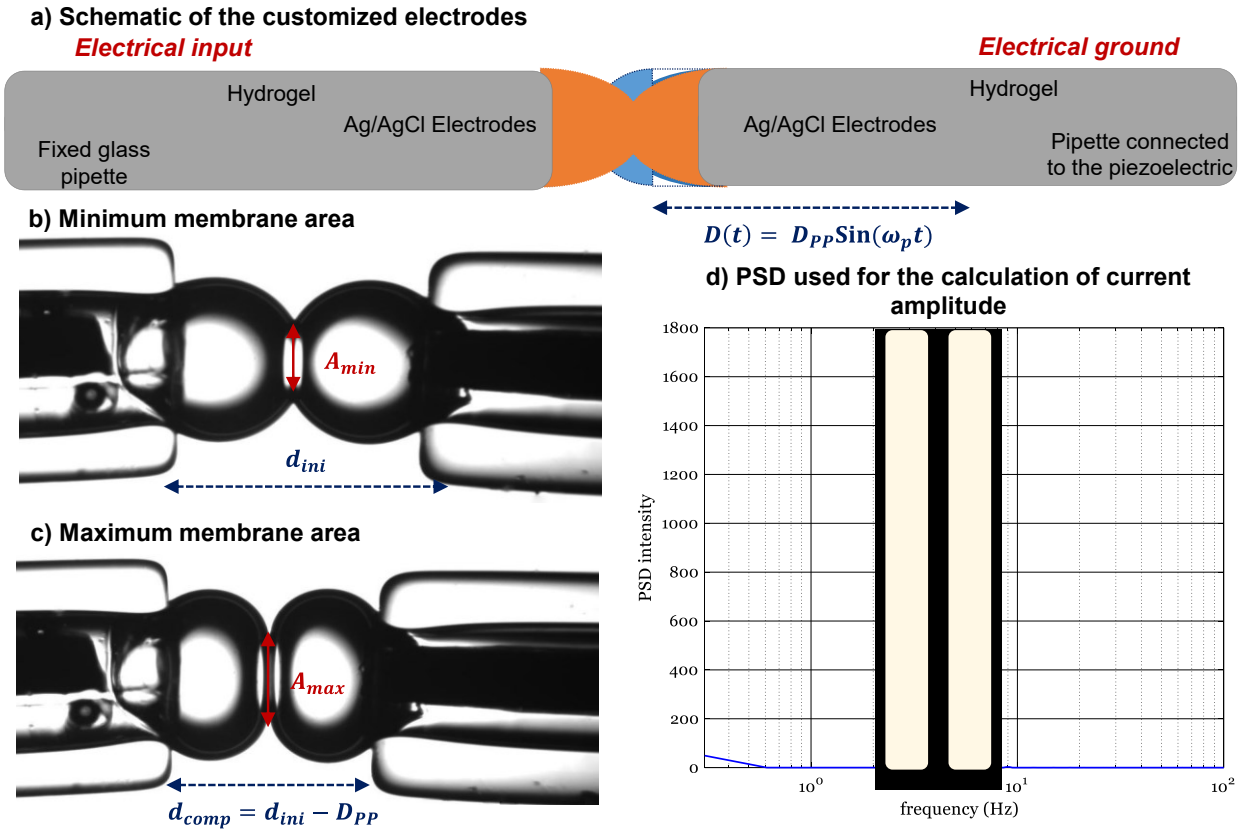

Figure 4. DIB customized experimental setup. a) Droplets containing lipids are placed on the tip of two parallel glass pipettes forming the lipid membrane at their adhered interface. The glass pipettes contain Ag/AgCl electrodes secured in place through hydrogels. The electrical ground pipette is attached to the piezoelectric actuator providing the mechanical displacement. b) and c) show the droplet compression leading to the membrane area expansion. This harmonic displacement is followed by a similar change in membrane area and thus capacitance, leading to the generation of mechanoelectricity. d) Power Spectral Density (PSD) of the generated mechanoelectric current is used to calculate its amplitude. The peak at the displacement frequency f_p (3 Hz) and at the second harmonic $2f_p$ (6 Hz) were both considered in the calculations.

The experimental platform adopted for generating mechanoelectricity is shown in **Figure 4 (a).** Two glass pipette electrodes are first prepared to hold the lipid-containing droplets [10, 52, 60, 61]. Silver/silver-chloride electrodes are then inserted into these cylindrical glass pipettes and fixed in place by filling the surrounding gaps with hydrogels. After solidifying the hydrogels, pipettes are submerged into a circular oil dish, while ensuring their parallel alignment for even compression. One pipette is connected to the headstage of an Axopatch 200B amplifier and remains immobile. The facing pipette is connected to the electrical ground and to the piezoelectric actuator. A function generator is used to provide the displacement of the piezoelectric actuator according to the following equation: $D(t) = D_{PP}\, sin\left(2\pi f_p t\right)$, where D_{PP} is the peak-to-peak amplitude and f_p is the oscillations frequency. This displacement induces a change in membrane area as seen in **Figure 4 (b) and (c).** The following parameters were adopted for all experiments shown in this work: D_{PP} = 150µm *and* f_p = 3Hz. This displacement amplitude was chosen as the one that generates a substantial current amplitude while avoiding excessive droplets perturbation or coalescence. This frequency value was selected as the optimum between excessive change in membrane tension [61] and accurate measurements of the mechanoelectric current [52]. More on the effect of displacement amplitude and frequency is discussed in **Sections S.4.2 and S.4.3. Figure 4 (d)** shows the power spectral density of the current signal, with clear peaks observed at the displacement's first and second frequencies, where the second frequency is associated with distortion of the original signal.

INSTRUMENTATION AND CONTROL DESIGN. A summary of the instrumentation and control design developed for membrane surface characterization is found in the supporting information, **Section S.4.4.** Briefly, a function generator is utilized to specify the displacement frequency and amplitude to the piezoelectric actuator (P601-Physik Instrumente) according to the

voltage-to-distance calibration. Upon initiating droplet compression, the mechanoelectric current is routed through the NI-cDAQ analogue input to a custom-designed LabVIEW VI. The fast Fourier transform (FFT) is generated through a sub-VI that calculates the amplitude and the phase angle of the current and the displacement. Based on these readings, the tuned PID controller calculates the necessary V_{DC} to minimize the mechanoelectric current, which is sent through the NI-cDAQ analogue output, and this voltage is recorded over time.

RESULTS AND DISCUSSIONS.

INITIAL TESTING OF THE CONTROL SYSTEM RESPONSE.

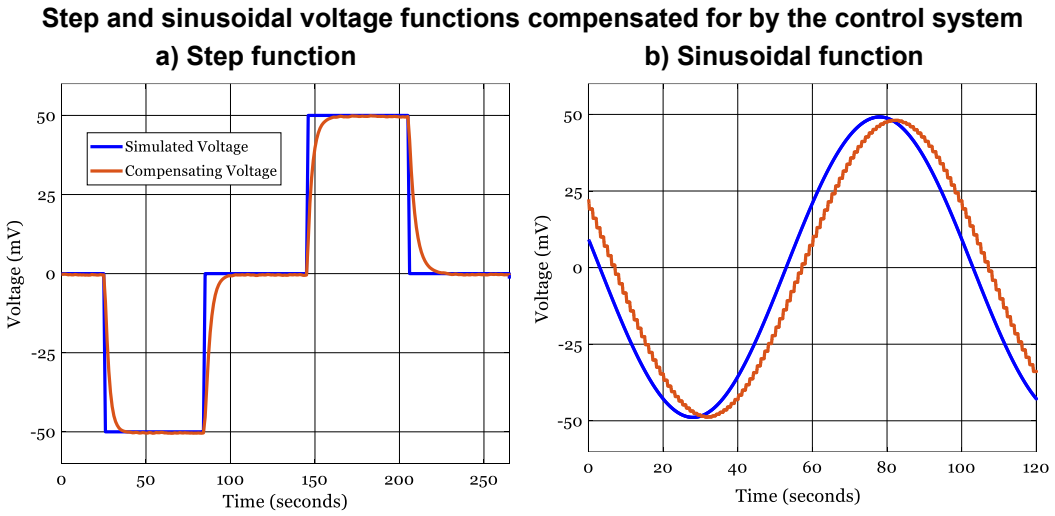

Figure 5. Simulated and compensating voltage showing the controller's response in tracking the membrane potential offset. An initially symmetric membrane, $\Delta\varphi \sim 0$ mV, was formed and a simulated a) step, and b) sinusoidal voltage functions were applied across the symmetric bilayer. Results show that the system is able to follow the applied voltage within few seconds lag and with least steady state error.

Prior to investigating transient membrane surface interactions, it is important to test and validate the reported compensating voltages provided by the mechanoelectricity technique. First, the

LabVIEW built-in PID controller was tuned, aiming for a short rise and settling time, while reducing overshoot and oscillations. For this fluidic system and for a hemisphere droplet size of approximately 1 mm in diameter submerged in hexadecane oil with the default oscillation parameters, the PID gains were calibrated as follows: $K_d = 10$, $T_i = 0.002$ and $T_d = 0.001$. Note that membrane dimensions and rate of response depend on experimental parameters and might influence the controller's performance. The tuned controller was then tested using an offset voltage provided by a function generator as shown in **Figure 5.** Results show that the steady state error is minimal, with an approximately 10-second lag between the tracked compensating voltage and the externally applied voltage. This lag may be reduced if necessary by increasing the compression frequency and reducing the cycles per measurement at the expense of precision and membrane stability.

FIXED MEMRBANE POTENTIAL OFFSET RESULTS.

a) Phospholipids with different surface and/or dipole potential

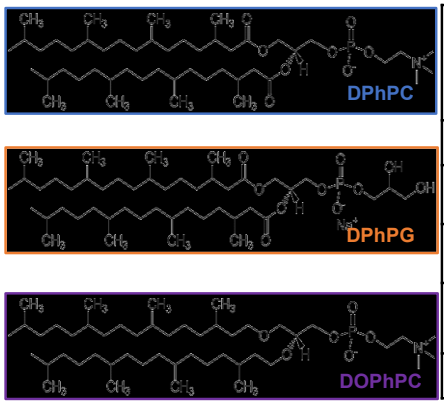

b) Membrane potential as calculated by the minimum capacitance technique and mechanoelectric (N≥5)

Input Side Leaflet	Ground Side Leaflet	Type of Asymmetry	Potential Offset (mV)	
			Minimum Capacitance	Mechano-electricity
DPhPC	DPhPC	None	- 0.5 (±3.2)	- 0.1 (±0.3)
DPhPC	DPhPG:DPhPC 1:4	Surface Potential Difference	26.5 (±3.1)	28.7 (±2.5)
DPhPG:DPhPC 1:4	DPhPC		-29.7 (±1.8)	- 32.0(±1.4)
DPhPC	DOPhPC	Dipole Potential Difference	125.8 (±2.5)	132.5 (±11)
DOPhPC	DPhPC		-133.0 (±4.3)	- 128.2 (±4.3)

Figure 6. Steady state membrane potential offset as measured by the traditional minimum capacitance technique [46] and mechanoelectricity. a) Three phospholipids are used herein as they present surface and dipole potential dissimilarities with respect to each other. DPhPC is a zwitterionic ester phospholipid, DPhPG is an anionic ester phospholipid and DOPhPC is a zwitterionic ether phospholipid. Molecular structures were obtained from Avanti Polar Lipids

(http://www.avantilipids.com). b) Symmetric membranes were formed with DPhPC/DPhPC; asymmetric membranes with surface potential difference were formed as DPhPC/1:4 DPhPG:DPhPC; asymmetric membranes with dipole potential difference were formed as DPhPC/DOPhPC. For asymmetric membranes, the electric field direction was switched by switching the sides of the monolayers with respect to the electrical input. This led to similar magnitude but opposite sign potentials. All experiments were conducted in hexadecane oil and for $N \geq 5$.

After verifying that the compensating voltage is able to follow a provided boundary potential as shown in **Figure 5**, we next move to measuring fixed offset asymmetric membranes. Three phospholipids were selected for generating asymmetric surface and dipole potentials as described in **Figure 6 (a)**. 1,2-diphytanoyl-sn-glycero-3-phosphocholine (DPhPC) is a zwitterionic ester phospholipid, used as a standard electrically neutral phospholipid. 1,2-diphytanoyl-sn-glycero-3-phospho-(1'-rac-glycerol) (sodium salt) (DPhPG) is an anionic ester phospholipid, when mixed with DPhPC the resulting monolayer presents an established negative surface charge that depends on the mass ratio of these two lipids as well as their area per lipid. The resulting monolayer presents a surface potential asymmetry with the zwitterionic DPhPC monolayer. Lastly, 1,2-di-O-phytanyl-sn-glycero-3-phosphocholine (DOPhPC) is a zwitterionic ether phospholipid, whose monolayer possesses a dipole potential difference in comparison to that of DPhPC.

Three membrane compositions were formed from these lipids as follows: symmetric DPhPC/DPhPC membranes, surface potential asymmetric DPhPC/1:4 DPhPG:DPhPC membranes, and dipole potential asymmetric DPhPC/DOPhPC membranes. The potential offsets of these three membranes using the established minimum capacitance technique [39, 41, 46] were compared to the values measured using mechanoelectricity. Note that the potential offsets of these

cases are expected to remain constant, as these membranes exhibit minimal lipids flip-flop [39], even under constant oscillations as confirmed in **Section S.6**.

For dipole asymmetric DPhPC/DOPhPC membranes, the potential offset obtained lies within the standard deviation of previously published work [39]. As for the surface asymmetric DPhPC/1:4 DPhPG:DPhPC membranes, the potential offset agrees with Grahame equation describing the surface potential [53], considering the ratio of anionic to zwitterionic phospholipids and the hydrating buffer solution described in **Section S.1.** Next, mechanoelectricity was utilized to measure the potential offset of these same membranes. Averages and standard deviations are shown in the table of **Figure 6 (b).** It is concluded that the potential offsets measured by mechanoelectricity align with those calculated from the minimum capacitance technique. Additional examples of these mechanoelectricity measurements are found in **Section S.5.**

CHARACTERIZING MEMBRANE-DETERGENTS SURFACE INTERACTIONS. The goal of this research is to identify membrane surface activities prior to membrane permeabilization through electrophysiology, which were previously undetected in measurements of membrane conductance. The interactions of disruptive agents at the membrane surface include the initial parallel surface attachment driven by electrostatic forces, followed by the transverse penetration driven by hydrophobic affinity [1]. These preliminary interactions are not observed in traditional conductance measurements. In the following two sections, we successfully track the transient processes of membrane permeabilization through the continuous and real-time detection of membrane surface activity initiated by slow-acting detergents, and a cationic antibacterial peptide.

First, symmetric membranes are formed, and rhythmic compressions are initiated using the piezoelectric actuator. At $t = 0$ seconds, a microdroplet containing the desired disruptive agent at a known concentration is added into the fixed droplet. The volume of the added microdroplet is

used to estimate the in-droplet concentration after equilibrium is reached. The compensating voltage is tracked over time until membrane permeabilization occurs i.e., sudden jumps in membrane conductance. While it is possible to continue the measurements of the offset voltage after the formation of pores, these jumps in the membrane conductance introduce excessive noise in the measured current which threaten the precision of the compensating voltage, even after appropriate modifications to remove the noise floor. Furthermore, since pore formation is linked to the agents traversing the membrane and interacting with both leaflets, the measured leaflet asymmetry is reduced after permeabilization and may no longer accurately link to the one-sided surface charge. Additional experimental details are found in **Section S.7 and S.8**.

The results showed herein showcase changes in the properties of the primary membrane formed between the electrodes, translated into changes in asymmetric surface charge [53]. The lipids-in technique, which is necessary for anionic and asymmetric membranes, was used consistently in all experiments, leading to an additional reservoir of lipid vesicles within the droplets themselves [14]. Consequently, while the permeabilization of the primary membrane is presented for all cases, this does not rule out additional interactions within the droplets themselves that are not detected using the technique.

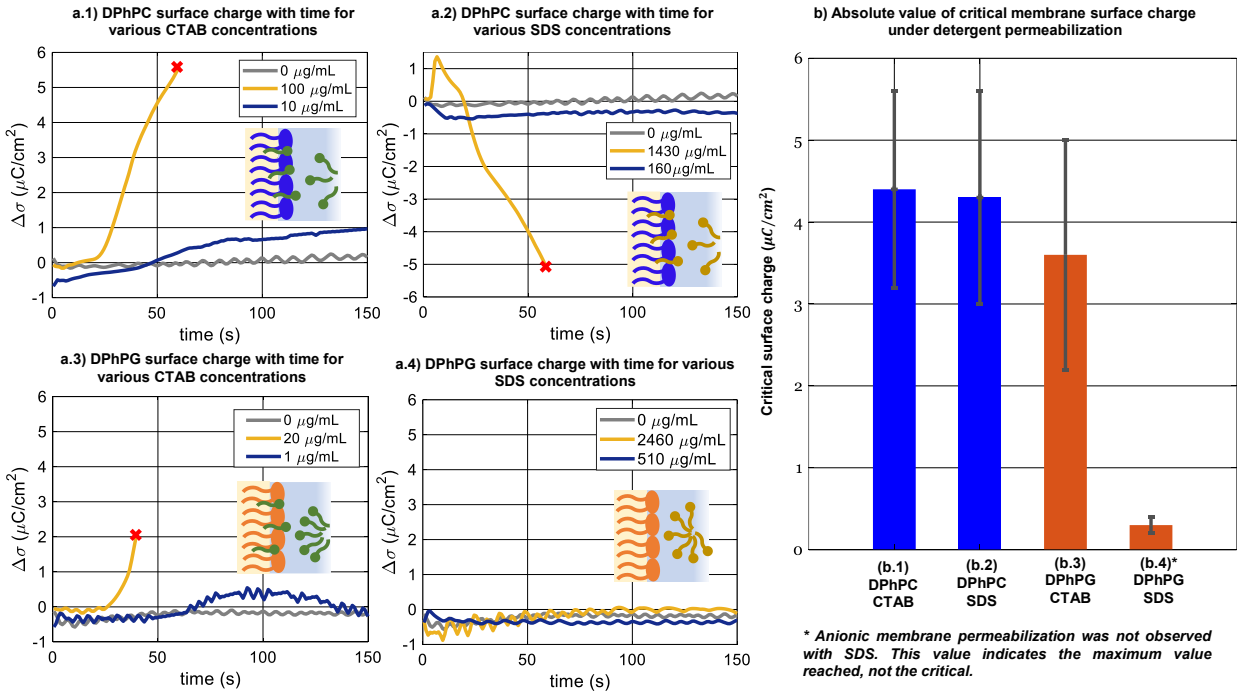

Figure 7. a) Example traces of membrane surface charge after injection of solubilizing detergents. Changes in the membrane surface charge with respect to time for neutral DPhPC and negatively charged 1:4 DPhPG:DPhPC membranes after injection of cationic CTAB and anionic SDS solubilizing detergents. Four cases were considered: a.1) DPhPC and CTAB, a.2) DPhPC and SDS, a.3) DPhPG and CTAB, a.4) DPhPG and SDS. For each case, three examples are shown here with varying detergent concentrations and behavior. The red marks indicate the beginning of membrane failure as observed through pore formation. Full results are found in Section SI.9. b) The change in surface charge right before the first sign of membrane degradation is denoted as the critical surface charge. The average and standard deviation of its absolute value are shown for each case. *Note that for the case of DPhPG and SDS (b.4), this surface charge indicates the maximum value reached rather than the critical one as these cases did not show any pore formation for more than 10 minutes observation.

Figure 7 shows the result of membrane-detergent interactions using the presented mechanoelectricity approach. Cationic CTAB and anionic SDS solubilizing detergents were selected for testing transient adsorption behaviors as they are well-characterized in the literature [6, 7, 54, 55]**.** The 4 membrane-detergent cases considered are: neutral DPhPC membranes with cationic CTAB detergent, neutral DPhPC with anionic SDS detergent, anionic 1:4 DPhPG:DPhPC membranes with cationic CTAB, and anionic 1:4 DPhPG:DPhPC with anionic SDS. In these plots, anionic membranes are denoted as "DPhPG" for simplicity, only the first 2.5 minutes of the recordings are shown, and the red marks indicate the start of membrane disruption at which the offset measurements are halted.

Plots shown in **Figure 7** provide representative examples, highlighting the difference in behavior depending on the membrane properties and detergent concentrations. **Figure 7 (a.1)** shows cationic CTAB disrupting DPhPC membranes. This case was observed over various detergent concentrations, where only the lowest concentration of $C_{CTAB} = 10\ \mu g/mL$ failed to solubilize the membrane. For higher concentrations, the critical surface charge required to initialize membrane permeability showed an average of $\Delta\sigma$ = + 4.4μC/cm^2 (± 1.2μC/cm^2) prior to disruption, as shown in **Figure 7 (b.1).** Following, **Figure 7 (a.2)** shows the effect of the anionic detergent SDS on these neutral membranes. Multiple detergent concentrations were adopted to test this interaction, out of which only C_{SDS}=160 μg/mL was unsuccessful at solubilizing the membrane even after 10 minutes. The remaining trials showed an average critical surface charge of $\Delta\sigma$ = - 4.3μC/cm^2 (± 1.3μC/cm^2), as shown in **Figure 7 (b.2**).

Figure 7 (a.3) shows CTAB solubilizing the negatively charged DPhPG membrane. Low concentration cases, $C_{CTAB} \leq 7\ \mu g/mL$, did not solubilize the membrane, rather a slight peak in membrane surface charge was observed, which after several minutes, converged back to the

original value. Higher concentrations lead to membrane solubilization with an average critical surface charge of $\Delta\sigma$ = + 3.6μC/cm^2 (± 1.4μC/cm^2), as shown in **Figure 7 (b.3)**. Finally, **Figure 7 (a.4)** shows the effect of anionic SDS detergents on DPhPG membranes. No interactions within the primary DIB membrane were observed in these cases. This is expected as the anionic detergent monomers are repelled from the negatively charged membrane surface.

Figure 7 (b) shows the average and standard deviations of the absolute value of the critical surface charge for each case. The critical surface charge is defined as the change in surface charge density right before membrane permeabilization, estimated through the offset potential. Absolute value was adopted simply to be able to compare cationic and anionic detergents noting that CTAB and SDS are both monovalent. Comparing the DPhPC cases for CTAB **(b.1)** and SDS **(b.2)**, the permeabilization of this electrically neutral membrane is less dependent on the concentration of detergent within the droplet but rather on the magnitude of the change in surface charge, or detergent accumulation. For both detergents, the average critical surface charge needed to initiate membrane permeabilization was similar (P(T<=t) two tail = 0.91), even where the SDS concentration within the droplet was typically an order of magnitude higher than the amount of CTAB necessary for permeabilization.

CTAB and SDS pinch off lipids from the exoplasmic layer prior to flipping into the inner leaflet and forming pores [55]. These interactions were observed prior to any membrane deterioration through mechanoelectricity as the detergents accumulated on one surface of the membrane before successfully forming pores. The data following initial pore formation is not shown in the plots of **Figure 7 (a)** as conductance variations are not a focus of this work but rather the surface activity that precedes them.

CHARACTERIZING MEMBRANE-MELITTIN SURFACE INTERACTIONS.

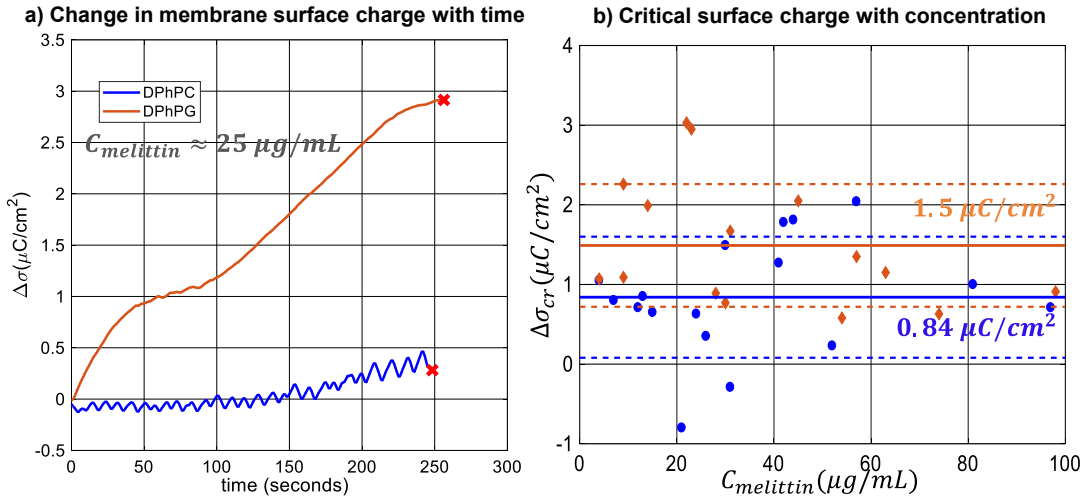

Figure 8. a) An example showing the change in membrane surface charge with melittin until membrane permeabilization, for electrically neutral membrane formed with zwitterionic DPhPC phospholipids, and negatively charged membrane formed with anionic 1:4 DPhPG:DPhPC lipids mixture. Red marks indicate the beginning of membrane degradation and data beyond this point was not considered. The surface charge right before initial membrane permeabilization is denoted as the critical surface charge. b) The critical surface charge is plotted with respect to various melittin concentrations. Solid lines indicate the average value for each membrane and the dashed lines indicate the range calculated considering the standard deviations. Detailed results are shown in Section S.10.

Investigating the activity of membrane-permeabilizing detergents in the previous section highlighted mechanoelectricity ability to detect accumulation prior to disruption. In this final section, similar experiments are conducted for the antimicrobial toxin, melittin [56, 58, 62-64]. Melittin is a cationic antimicrobial peptide that permeabilizes membranes [56, 58, 64, 65], while showing different disruption mechanisms depending on the membrane electrostatics [59, 62, 66].

Herein, we utilize mechanoelectricity to examine these differences in melittin surface accumulation prior to permeabilization with varying membrane compositions.

Multiple experiments were conducted with neutral and anionic membranes, while varying melittin concentration. A total of *N*=21 and *N*=23 trials were conducted with DPhPC and DPhPG membranes, respectively. Out of which, *N*=4 (of DPhPC) and *N*=8 (of DPhPG) showed no permeabilization of the primary DIB membrane within 10 minutes of observations. The remaining cases showed membrane disruption leading to total failure and only these experiments were considered in our calculations. Detailed results are found in **Section S.10.**

Figure 8 (a) shows an example of the change in membrane surface charge density with respect to time for $C_{melittin}$ ~ 25μg/mL comparing DPhPC and DPhPG membranes. Note the amplified surface activity induced by melittin on the anionic surface compared to the neutral case. In this specific example, similar time was needed to initiate permeabilization, noting that this is a happenstance and was not the case for all experiments. The red marks indicate the onset of membrane poration and the corresponding surface charge was denoted as the critical surface charge and obtained for all experiments and shown in **Figure 8 (b).** The dashed lines indicate the average value for all cases of each membrane: $\sigma_{cr} = 0.84\ \mu C/cm^2$ ($\pm 0.76 \mu C/cm^2$) was calculated for neutral membranes, compared to an average of $\sigma_{cr} = 1.5\ \mu C/cm^2$ ($\pm 0.77 \mu C/cm^2$) for anionic membranes. This significant difference (P(T<=t) two tail = 0.02) in the surface accumulation of melittin between neutral and anionic membranes prior to the formation of pores reinforces literature findings [59, 62, 66-68], noting that anionic membranes have been observed to be more resistant to melittin permeabilization [59, 66]. Our results further support this understanding as 19% of DPhPC membranes resisted permeabilization compared to 35% of DPhPG membranes. The electrostatic attraction between the cationic peptide and the anionic

membrane surface drives melittin to rapidly accumulate onto the membrane leading to a surface dominant behavior that is not observed in the case of neutral membranes [59]. A higher surface charge value indicates more peptide accumulation on the membrane leaflets as previously described in **Figure 2 (c).** Furthermore, the average presented in **Figure 8 (b)** can be translated into peptide-to-lipid ratio considering the charge of melittin [68] and the area per lipid of these phospholipids [69]: $P/L^{*}\sim 0.015$ and 0.0085 for anionic and neutral membranes, respectively. The literature presents this characteristic in various studies [64, 65, 67, 68]. Specifically, Benachir *et al.,* showed that a $P/L = 0.004$ is needed to significantly permeabilize neutral liposomes, and this value increased to $P/L = 0.03$ when 30% anionic phospholipids were added [67]. Our results produce a similar trend, while measuring accumulation prior to pore formation rather than vesicle leakage.

CONCLUSION. This manuscript investigates the use of mechanoelectricity for tracking membrane disruption prior to pore formation. The approach involves exploitation of the liquid-in-liquid nature of the droplet interface bilayer for the generation of capacitance-induced mechanoelectric current based on the voltage drop across the membrane. Continuous minimization of this current via a customized control system produces measurements of membrane disruption previously hidden in electrophysiology studies. The innovation of this approach lies within its ability to characterize membrane-agent interactions in real-time prior to membrane permeabilization.

The technique was validated against electrowetting results using asymmetric lipid membranes. Next, the technique was applied towards characterizing detergent-membrane interactions for cationic and anionic model detergents. The accumulation immediately prior to pore formation for both detergents was comparable, and the technique is able to distinguish between membrane

accumulation and the concentration in the solution. Finally, the technique was applied towards the interaction of melittin within lipid membranes confirming that the peptide's insertion mechanics are modulated by membrane composition.

In each of the presented measurements for membrane accumulation the produced values are obtained prior to the formation of conductive pores. These are changes in the membrane properties that are often invisible in standard electrophysiological recordings because they are not reflected in the membrane conductance or capacitance. The mechanoelectric technique permits for measurements of membrane accumulation that may be combined with standard measurements of pore formation and provides another tool to investigate membrane permeabilization in greater detail. Future research using this approach may be used to resolve crucial first steps in membrane-aided disruption for topics ranging from targeted antimicrobial development to optimizing drug delivery vectors.

ASSOCIATED CONTENT. Supplementary information is attached and includes materials and methods for the experimental setup and optimization of mechanoelectricity and additional results details.

AUTHOR INFORMATION

Corresponding Author

***Eric Freeman –** Biomembranes Engineering Laboratory, School of Environmental, Civil, Agricultural and Mechanical Engineering, The University of Georgia, Athens, GA 30602, ecfreema@uga.edu

Authors

Joyce El-Beyrouthy – Biomembranes Engineering Laboratory, School of Environmental, Civil, Agricultural and Mechanical Engineering, The University of Georgia, Athens, GA 30602, joyce.elbeyrouthy@uga.edu

Michelle M. Makhoul-Mansour – Biomembranes Engineering Laboratory, School of Environmental, Civil, Agricultural and Mechanical Engineering, The University of Georgia, Athens, GA 30602, michelle.mansour55@uga.edu

Author Contributions

J.E. carried out the experimental work, participated in data analysis, participated in the design of the study and drafted the manuscript. M.M. participated in the design of the study and critically revised the manuscript. E.F. conceived of the study, coordinated the study, participated in data analysis and design of the study and helped draft the manuscript. All authors gave final approval for publication and agree to be held accountable for the work performed therein.

Funding Sources

The authors gratefully acknowledge support from the National Science Foundation (NSF) under grant no. 1903965.

REFERENCES

1. Jenssen, H., Hamill, P., and Hancock, R.E., *Peptide Antimicrobial Agents.* Clinical microbiology reviews, 2006. **19**(3): p. 491-511.

2. Peetla, C., Bhave, R., Vijayaraghavalu, S., Stine, A., Kooijman, E., and Labhasetwar, V.J.M.p., *Drug Resistance in Breast Cancer Cells: Biophysical Characterization of and Doxorubicin Interactions with Membrane Lipids.* 2010. **7**(6): p. 2334-2348.

3. Simelane, L.P., Fosso-Kankeu, E., Njobeh, P., and Pandey, S.J.C.S., *Response of Bacterial Biosorbents to Chemical Treatment as Influenced by Cell Membrane Structure and Impact on the Adsorption Behaviour of Dyes.* 2018. **114**(4): p. 826-834.

4. Fröhlich, E.J.I.j.o.n., *The Role of Surface Charge in Cellular Uptake and Cytotoxicity of Medical Nanoparticles.* 2012. **7**: p. 5577.

5. Chamundeeswari, M., Jeslin, J., and Verma, M.L.J.E.C.L., *Nanocarriers for Drug Delivery Applications.* 2019. **17**(2): p. 849-865.

6. Vaidyanathan, S., Orr, B.G., and Banaszak Holl, M.M.J.T.J.o.P.C.B., *Detergent Induction of Hek 293a Cell Membrane Permeability Measured under Quiescent and Superfusion Conditions Using Whole Cell Patch Clamp.* 2014. **118**(8): p. 2112-2123.

7. Pata, V., Ahmed, F., Discher, D.E., and Dan, N.J.L., *Membrane Solubilization by Detergent: Resistance Conferred by Thickness.* 2004. **20**(10): p. 3888-3893.

8. Jain, K., Kesharwani, P., Gupta, U., and Jain, N.J.I.j.o.p., *Dendrimer Toxicity: Let's Meet the Challenge.* 2010. **394**(1-2): p. 122-142.

9. Majd, S., Yusko, E.C., Billeh, Y.N., Macrae, M.X., Yang, J., and Mayer, M.J.C.O.i.B., *Applications of Biological Pores in Nanomedicine, Sensing, and Nanoelectronics.* 2010. **21**(4): p. 439-476.

10. Kancharala, A., Freeman, E., Philen, M.J.S.M., and Structures, *A Comprehensive Flexoelectric Model for Droplet Interface Bilayers Acting as Sensors and Energy Harvesters.* 2016. **25**(10): p. 104007.

11. Korn, E.D.J.S., *Structure of Biological Membranes.* 1966. **153**(3743): p. 1491-1498.

12. Malanovic, N. and Lohner, K.J.B.e.B.A.-B., *Gram-Positive Bacterial Cell Envelopes: The Impact on the Activity of Antimicrobial Peptides.* 2016. **1858**(5): p. 936-946.

13. Shai, Y.J.B.e.B.A.-B., *Mechanism of the Binding, Insertion and Destabilization of Phospholipid Bilayer Membranes by A-Helical Antimicrobial and Cell Non-Selective Membrane-Lytic Peptides.* 1999. **1462**(1-2): p. 55-70.

14. El-Beyrouthy, J. and Freeman, E., *Characterizing the Structure and Interactions of Model Lipid Membranes Using Electrophysiology.* 2021. **11**(5): p. 319.

15. Bunea, A.-I., Harloff-Helleberg, S., Taboryski, R., Nielsen, H.M.J.A.i.c., and science, i., *Membrane Interactions in Drug Delivery: Model Cell Membranes and Orthogonal Techniques.* 2020. **281**: p. 102177.

16. Al Nahas, K. and Keyser, U.F.J.B., *Standardizing Characterization of Membrane Active Peptides with Microfluidics.* 2021. **15**(4): p. 041301.

17. Tsemperouli, M., Amstad, E., Sakai, N., Matile, S., and Sugihara, K.J.L., *Black Lipid Membranes: Challenges in Simultaneous Quantitative Characterization by Electrophysiology and Fluorescence Microscopy.* 2019. **35**(26): p. 8748-8757.

18. Sezgin, E.J.J.o.P.C.M., *Super-Resolution Optical Microscopy for Studying Membrane Structure and Dynamics.* 2017. **29**(27): p. 273001.

19. Wallner, J., Lhota, G., Jeschek, D., Mader, A., Vorauer-Uhl, K.J.J.o.p., and analysis, b., *Application of Bio-Layer Interferometry for the Analysis of Protein/Liposome Interactions.* 2013. **72**: p. 150-154.

20. Luchini, A., Gerelli, Y., Fragneto, G., Nylander, T., Pálsson, G.K., Appavou, M.-S., Paduano, L.J.C., and Biointerfaces, S.B., *Neutron Reflectometry Reveals the Interaction between Functionalized Spions and the Surface of Lipid Bilayers.* 2017. **151**: p. 76-87.

21. Biswas, N., Bhattacharya, R., Saha, A., Jana, N.R., and Basu, J.K.J.P.C.C.P., *Interplay of Electrostatics and Lipid Packing Determines the Binding of Charged Polymer Coated Nanoparticles to Model Membranes.* 2015. **17**(37): p. 24238-24247.

22. Rusciano, G., De Luca, A., Pesce, G., and Sasso, A.J.C., *On the Interaction of Nano-Sized Organic Carbon Particles with Model Lipid Membranes.* 2009. **47**(13): p. 2950-2957.

23. Li, Y., Chen, X., and Gu, N.J.T.J.o.P.C.B., *Computational Investigation of Interaction between Nanoparticles and Membranes: Hydrophobic/Hydrophilic Effect.* 2008. **112**(51): p. 16647-16653.

24. Lee, O.-S. and Schatz, G.C., *Computational Simulations of the Interaction of Lipid Membranes with DNA-Functionalized Gold Nanoparticles*, in *Biomedical Nanotechnology*. 2011, Springer. p. 283-296.

25. Sekiya, Y., Shimizu, K., Kitahashi, Y., Ohyama, A., Kawamura, I., and Kawano, R.J.A.A.B.M., *Electrophysiological Analysis of Membrane Disruption by Bombinin and Its Isomer Using the Lipid Bilayer System.* 2019. **2**(4): p. 1542-1548.

26. Hancock, R.E. and Rozek, A., *Role of Membranes in the Activities of Antimicrobial Cationic Peptides.* FEMS microbiology letters, 2002. **206**(2): p. 143-149.

27. Kagan, B.L., Selsted, M.E., Ganz, T., and Lehrer, R.I.J.P.o.t.N.A.o.S., *Antimicrobial Defensin Peptides Form Voltage-Dependent Ion-Permeable Channels in Planar Lipid Bilayer Membranes.* 1990. **87**(1): p. 210-214.

28. Wu, M., Maier, E., Benz, R., and Hancock, R.E., *Mechanism of Interaction of Different Classes of Cationic Antimicrobial Peptides with Planar Bilayers and with the Cytoplasmic Membrane of Escherichia Coli.* Biochemistry, 1999. **38**(22): p. 7235-7242.

29. Schoch, P., Sargent, D.F., and Schwyzer, R., *Capacitance and Conductance as Tools for the Measurement of Asymmetric Surface Potentials and Energy Barriers of Lipid Bilayer Membranes.* The Journal of Membrane Biology, 1979. **46**(1): p. 71-89.

30. Fuks, B. and Homble, F.J.B.j., *Permeability and Electrical Properties of Planar Lipid Membranes from Thylakoid Lipids.* 1994. **66**(5): p. 1404-1414.

31. Alvarez, O. and Latorre, R., *Voltage-Dependent Capacitance in Lipid Bilayers Made from Monolayers.* Biophysical journal, 1978. **21**(1): p. 1-17.

32. Hamill, O.P., Marty, A., Neher, E., Sakmann, B., and Sigworth, F.J.P.A., *Improved Patch-Clamp Techniques for High-Resolution Current Recording from Cells and Cell-Free Membrane Patches.* 1981. **391**(2): p. 85-100.

33. Montal, M. and Mueller, P., *Formation of Bimolecular Membranes from Lipid Monolayers and a Study of Their Electrical Properties.* Proceedings of the National Academy of Sciences, 1972. **69**(12): p. 3561-3566.

34. Cevc, G., *Membrane Electrostatics.* Biochimica et Biophysica Acta (BBA)-Reviews on Biomembranes, 1990. **1031**(3): p. 311-382.

35. Kinraide, T.B.J.P.P., *Use of a Gouy-Chapman-Stern Model for Membrane-Surface Electrical Potential to Interpret Some Features of Mineral Rhizotoxicity.* 1994. **106**(4): p. 1583-1592.

36. Clarke, R.J.J.A.i.c. and science, i., *The Dipole Potential of Phospholipid Membranes and Methods for Its Detection.* 2001. **89**: p. 263-281.

37. Sokolov, V. and Mirsky, V., *Electrostatic Potentials of Bilayer Lipid Membranes: Basic Principles and Analytical Applications*, in *Ultrathin Electrochemical Chemo-and Biosensors*. 2004, Springer. p. 255-291.

38. Pohl, E.E., Peterson, U., Sun, J., and Pohl, P., *Changes of Intrinsic Membrane Potentials Induced by Flip-Flop of Long-Chain Fatty Acids.* Biochemistry, 2000. **39**(7): p. 1834-1839.

39. Taylor, G., Nguyen, M.-A., Koner, S., Freeman, E., Collier, C.P., and Sarles, S.A., *Electrophysiological Interrogation of Asymmetric Droplet Interface Bilayers Reveals Surface-*

Bound Alamethicin Induces Lipid Flip-Flop. Biochimica et Biophysica Acta (BBA)-Biomembranes, 2018.

40. El-Beyrouthy, J., Makhoul-Mansour, M.M., Taylor, G., Sarles, S.A., and Freeman, E.C., *A New Approach for Investigating the Response of Lipid Membranes to Electrocompression by Coupling Droplet Mechanics and Membrane Biophysics.* Journal of the Royal Society Interface, 2019. **16**(161): p. 20190652.

41. Makhoul-Mansour, M.M., El-Beyrouthy, J.B., Mumme, H.L., and Freeman, E.C., *Photopolymerized Microdomains in Both Lipid Leaflets Establish Diffusive Transport Pathways across Biomimetic Membranes.* Soft matter, 2019. **15**(43): p. 8718-8727.

42. Heimburg, T., *The Capacitance and Electromechanical Coupling of Lipid Membranes Close to Transitions: The Effect of Electrostriction.* Biophysical journal, 2012. **103**(5): p. 918-929.

43. Passechnik, V.I. and Sokolov, V.S.J.B., *Estimation of Electrochrome Dyes Position in the Bilayer through the 2nd Harmonic of Capacitive Current.* 2002. **55**(1-2): p. 47-51.

44. Sokolov, V., Chernyi, V., and Markin, V.J.B., *Measurement of Potential Jumps on Adsorption of Phloretin and Phlorezin on the Surface of Lipid Membranes by the Intramembrane Field Compensation Method.* 1984. **29**(3): p. 464-470.

45. Sokolov, V. and Kuz'min, V.J.B., *Measurement of the Difference in the Surface Potentials of Bilayer Membranes from the Second Harmonic of the Capacitance Current.* 1980. **25**(1): p. 174-177.

46. El-Beyrouthy, J. and Freeman, E.C. *Rapid and Real-Time Measurement of Membrane Potential through Intramembrane Field Compensation*. in *Smart Materials, Adaptive Structures and Intelligent Systems*. 2020. American Society of Mechanical Engineers.

47. Gross, L.C., Heron, A.J., Baca, S.C., and Wallace, M.I., *Determining Membrane Capacitance by Dynamic Control of Droplet Interface Bilayer Area.* Langmuir, 2011. **27**(23): p. 14335-14342.

48. Berthier, J. and Brakke, K., *The Physics of Microdrops.* Scrivener-Wiley publishing. doi, 2012. **10**: p. 9781118401323.

49. Challita, E.J., Makhoul-Mansour, M.M., and Freeman, E.C.J.B., *Reconfiguring Droplet Interface Bilayer Networks through Sacrificial Membranes.* 2018. **12**(3): p. 034112.

50. Bayley, H., Cronin, B., Heron, A., Holden, M.A., Hwang, W.L., Syeda, R., Thompson, J., and Wallace, M., *Droplet Interface Bilayers.* Mol Biosyst, 2008. **4**(12): p. 1191-1208.

51. Poulin, P. and Bibette, J., *Adhesion of Water Droplets in Organic Solvent.* Langmuir, 1998. **14**(22): p. 6341-6343.

52. Freeman, E.C., Najem, J.S., Sukharev, S., Philen, M.K., and Leo, D.J., *The Mechanoelectrical Response of Droplet Interface Bilayer Membranes.* Soft Matter, 2016. **12**(12): p. 3021-3031.

53. Grahame, D.C.J.C.r., *The Electrical Double Layer and the Theory of Electrocapillarity.* 1947. **41**(3): p. 441-501.

54. Lichtenberg, D., Ahyayauch, H., and Goñi, F.M.J.B.j., *The Mechanism of Detergent Solubilization of Lipid Bilayers.* 2013. **105**(2): p. 289-299.

55. Lete, M.G., Monasterio, B.G., Collado, M.I., Medina, M., Sot, J., Alonso, A., Goñi, F.M.J.C., and Biointerfaces, S.B., *Fast and Slow Biomembrane Solubilizing Detergents: Insights into Their Mechanism of Action.* 2019. **183**: p. 110430.

56. Allende, D., Simon, S., and McIntosh, T.J.J.B.j., *Melittin-Induced Bilayer Leakage Depends on Lipid Material Properties: Evidence for Toroidal Pores.* 2005. **88**(3): p. 1828-1837.

57. Liu, J., Xiao, S., Li, J., Yuan, B., Yang, K., and Ma, Y.J.B.e.B.A.-B., *Molecular Details on the Intermediate States of Melittin Action on a Cell Membrane.* 2018. **1860**(11): p. 2234-2241.

58. Yang, L., Harroun, T.A., Weiss, T.M., Ding, L., and Huang, H.W.J.B.j., *Barrel-Stave Model or Toroidal Model? A Case Study on Melittin Pores.* 2001. **81**(3): p. 1475-1485.

59. Pandidan, S. and Mechler, A.J.S.r., *Nano-Viscosimetry Analysis of the Membrane Disrupting Action of the Bee Venom Peptide Melittin.* 2019. **9**(1): p. 1-12.

60. Najem, J.S., Dunlap, M.D., Rowe, I.D., Freeman, E.C., Grant, J.W., Sukharev, S., and Leo, D.J., *Activation of Bacterial Channel Mscl in Mechanically Stimulated Droplet Interface Bilayers.* Sci Rep, 2015. **5**: p. 13726.

61. Najem, J.S., Freeman, E.C., Yasmann, A., Sukharev, S., and Leo, D.J.J.A.M.I., *Mechanics of Droplet Interface Bilayer "Unzipping" Defines the Bandwidth for the Mechanotransduction Response of Reconstituted Mscl.* 2017. **4**(3): p. 1600805.

62. Lee, T.H., Mozsolits, H., and Aguilar, M.I.J.T.J.o.p.r., *Measurement of the Affinity of Melittin for Zwitterionic and Anionic Membranes Using Immobilized Lipid Biosensors.* 2001. **58**(6): p. 464-476.

63. Van Den Bogaart, G., Guzmán, J.V., Mika, J.T., and Poolman, B.J.J.o.B.C., *On the Mechanism of Pore Formation by Melittin.* 2008. **283**(49): p. 33854-33857.

64. Lee, M.-T., Sun, T.-L., Hung, W.-C., and Huang, H.W.J.P.o.t.N.A.o.S., *Process of Inducing Pores in Membranes by Melittin.* 2013. **110**(35): p. 14243-14248.

65. Huang, H.W.J.B.j., *Free Energies of Molecular Bound States in Lipid Bilayers: Lethal Concentrations of Antimicrobial Peptides.* 2009. **96**(8): p. 3263-3272.

66. Strömstedt, A.A., Wessman, P., Ringstad, L., Edwards, K., Malmsten, M.J.J.o.c., and science, i., *Effect of Lipid Headgroup Composition on the Interaction between Melittin and Lipid Bilayers.* 2007. **311**(1): p. 59-69.

67. Benachir, T. and Lafleur, M.J.B.e.B.A.-B., *Study of Vesicle Leakage Induced by Melittin.* 1995. **1235**(2): p. 452-460.

68. Ohki, S., Marcus, E., Sukumaran, D.K., and Arnold, K.J.B.e.B.A.-B., *Interaction of Melittin with Lipid Membranes.* 1994. **1194**(2): p. 223-232.

69. Yasmann, A. and Sukharev, S., *Properties of Diphytanoyl Phospholipids at the Air–Water Interface.* Langmuir, 2014. **31**(1): p. 350-357.

ToC

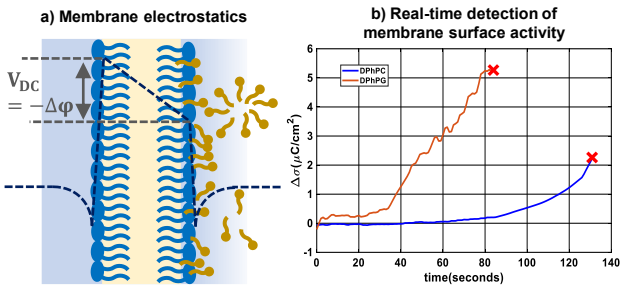
a) Membrane electrostatics
V_{DC}
$= -\Delta\varphi$
b) Real-time detection of membrane surface activity
DPhPC
DPhPG
$\Delta\sigma$ (μC/cm^2)
time(seconds)
0
20
40
60
80
100
120
140
-1
0
1
2
3
4
5
6